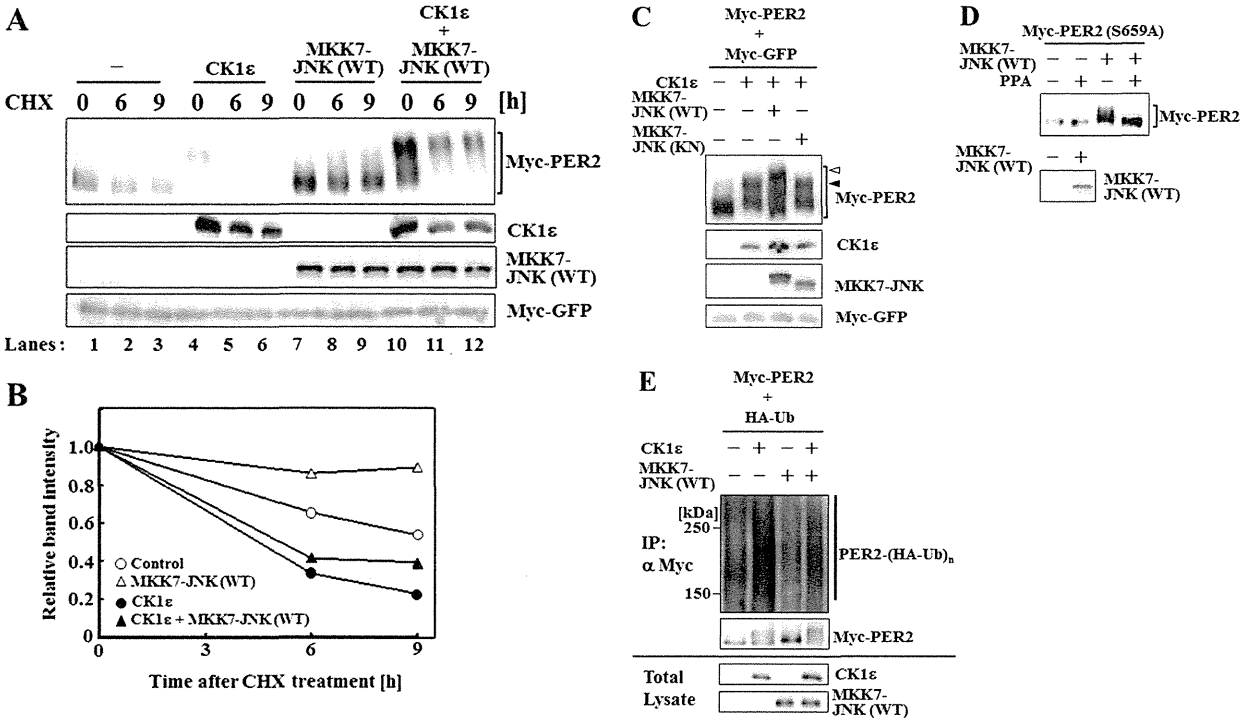

FIGURE 5. **MKK7-activated JNK inhibits CK1ε-mediated PER2 degradation.** *A*, effect of CHX. 293T cells were transfected with vectors expressing Myc-PER2 and Myc-GFP, plus empty vector (−), CK1ε, or MKK7-JNK (WT) alone or in combination, as indicated. Transfected cells were treated with 20 μg/ml CHX at time 0. At the indicated times after CHX treatment, protein extracts were analyzed by WB with anti-Myc, anti-CK1, or anti-JNK Ab to detect Myc-PER2 and Myc-GFP, CK1ε, and MKK7-JNK (WT) proteins, respectively. *B*, quantitation of *A*. Relative band intensities in the blot in *A* were determined and analyzed as for Fig. 4*C*. *C*, mobility shift of PER2. 293T cells were transfected with vectors expressing Myc-PER2 and Myc-GFP plus either empty vector, MKK7-JNK (WT), MKK7-JNK (KN), or CK1ε, as indicated. Protein extracts were analyzed by WB with anti-Myc, anti-CK1, and anti-JNK. The *black arrowhead* indicates the band shift induced by co-expression of CK1ε; the *white arrowhead* indicates the band supershift induced by co-expression of CK1ε and MKK7-JNK (WT). *D*, sensitivity to phosphatase. *Top*, HeLa cells were co-transfected with vector expressing Myc-PER2 (S659A) plus either empty vector (−) or vector expressing MKK7-JNK (WT) (+). Myc-PER2 (S659A) was immunoprecipitated with anti-Myc Ab, treated (+) or not (−) with alkaline phosphatase (*PPA*), and analyzed by WB with anti-Myc Ab. *Bottom*, MKK7-JNK (WT) was detected by WB with anti-JNK Ab. *E*, MKK7-JNK suppresses CK1ε-induced PER2 ubiquitination. 293T cells were transfected with Myc-PER2 and HA-Ub plus empty vector (−), MKK7-JNK (WT), or CK1ε alone or in combination, as indicated. *Top*, lysates were immunoprecipitated (*IP*) with anti-Myc Ab and subjected to WB analysis with anti-HA Ab to detect ubiquitinated PER2 (*PER2-(HA-Ub)$_n$*). *Middle*, lysates were immunoprecipitated with anti-Myc Ab and analyzed by WB using anti-Myc Ab to detect Myc-PER2. *Bottom*, total cell lysates were analyzed by WB using anti-JNK (MKK7-JNK) or anti-CK1ε (CK1ε) Abs.

First, the MKK7-JNK (WT) fusion protein, which is a constitutively active form of JNK, can phosphorylate PER2 (Fig. 2). Importantly, the threonines in the consensus JNK phosphorylation motifs present in PER2 were phosphorylated in cultured cells, and co-expression of MKK7-JNK (WT) enhanced this phosphorylation (Fig. 2*E*). Second, we showed that JNK interacts with PER2 at both the exogenous and endogenous levels (Fig. 3). Third, overexpression of MKK7-JNK (WT) inhibited PER2 ubiquitination and stabilized PER2 protein (Fig. 4). These results, together with our observation that the genetic inactivation of MKK7 has an influence on circadian gene expression (Fig. 1), suggest that the MKK7-JNK pathway contributes to circadian rhythm regulation by controlling PER2 protein levels and thus PER2 functions.

Many kinases, including CK1ε, CK1δ, CK2, and GSK3β, have been shown to regulate PER2 functions (13, 14, 17, 36, 37). Moreover, these kinases can cooperate in this regard because CK2 reportedly decreases PER2 protein stability by enhancing CK1ε-mediated PER2 degradation (36). In our study, we found that co-expression of MKK7-JNK (WT) decreased CK1ε-mediated PER2 degradation (Fig. 5). However, our data show that MKK7-JNK signaling does not directly inhibit CK1ε-mediated PER2 phosphorylation and may instead phosphorylate PER2 residue(s) different from those targeted by CK1ε-dependent phosphorylation. In short, MKK7-JNK signaling and CK1ε appear to have opposing regulatory effects on PER2 protein stability that are mediated via differential phosphorylation. Future studies should establish how the MKK7-JNK cascade combines with other kinases either to control the oscillatory mechanism itself or to modulate the signaling pathway that drives circadian entrainment in response to external signals.

The control of PER2 stability via phosphorylation is associated with the period length of circadian gene expression (19, 20). Notably, the phosphorylation of PER2 protein regulates its stability in multiple ways, and this phosphorylation depends both on which phosphorylation sites are used and on which kinases are performing the phosphorylation (12, 13). In addition, interference with phosphorylation-dependent PER2 stability controls can lead to either short or long circadian periods, making it difficult to predict how a given level of PER2 stability will affect the period length of circadian gene expression (18–20, 37, 38). For example, both mutation of PER2 Ser-662, which leads to a lower rate of CK1ε/δ-dependent phosphorylation, and mutation of PER2 N-terminal phosphoacceptor sites for CK2 lead to PER2 instability. However, these mutations have the opposite effect on the circadian period; Ser-662 mutation

shortens the period, whereas N-terminal mutation extends it (19, 20, 37). Thus, further elucidation of the processes that affect PER2 stability are required to unravel the complex and largely mysterious post-translational controls governing circadian timing in mammals.

Previous work has established that a single kinase is capable of phosphorylating multiple clock components (13, 14). For example, CK1ε can phosphorylate PER1, PER2, PER3, BMAL1, and CRY1, altering their subcellular localization, protein stability, and transcriptional activity and thus contributing to regulation of their functions (17, 39–41). Our results indicate that, in addition to PER2, BMAL1 is also a target for MKK7-JNK-mediated phosphorylation. We have not yet obtained enough data to prove that BMAL1 phosphorylation is required for circadian clock function, and the physiological importance of this phosphorylation remains under investigation.

In addition to their circadian clock functions, PER2 and BMAL1 participate in non-circadian physiological processes, such as tumor suppression (34), aging (42), immune responses (43), and metabolic control (44–46). MKK7-JNK-dependent phosphorylation of circadian regulators, such as PER2 and BMAL1, may therefore be a key integrating event that translates internal and external signals into a variety of physiological cellular responses, including circadian rhythm adjustment.

Acknowledgments—We are grateful to all members of the Nishina and Katada laboratories (Tokyo University) for insightful comments.

REFERENCES

1. Davis, R. J. (2000) Signal transduction by the JNK group of MAP kinases. *Cell* **103,** 239–252
2. Chang, L., and Karin, M. (2001) Mammalian MAP kinase signaling cascades. *Nature* **410,** 37–40
3. Lawler, S., Fleming, Y., Goedert, M., and Cohen, P. (1998) Synergistic activation of SAPK1/JNK1 by two MAP kinase kinases *in vitro*. *Curr. Biol.* **8,** 1387–1390
4. Kishimoto, H., Nakagawa, K., Watanabe, T., Kitagawa, D., Momose, H., Seo, J., Nishitai, G., Shimizu, N., Ohata, S., Tanemura, S., Asaka, S., Goto, T., Fukushi, H., Yoshida, H., Suzuki, A., Sasaki, T., Wada, T., Penninger, J. M., Nishina, H., and Katada, T. (2003) Different properties of SEK1 and MKK7 in dual phosphorylation of stress-induced activated protein kinase SAPK/JNK in embryonic stem cells. *J. Biol. Chem.* **278,** 16595–16601
5. Pizzio, G. A., Hainich, E. C., Ferreyra, G. A., Coso, O. A., and Golombek, D. A. (2003) Circadian and photic regulation of ERK, JNK, and p38 in the hamster SCN. *Neuroreport* **14,** 1417–1419
6. Chansard, M., Molyneux, P., Nomura, K., Harrington, M. E., and Fukuhara, C. (2007) c-Jun N-terminal kinase inhibitor SP600125 modulates the period of mammalian circadian rhythms. *Neuroscience* **145,** 812–823
7. Wada, T., Joza, N., Cheng, H. Y., Sasaki, T., Kozieradzki, I., Bachmaier, K., Katada, T., Schreiber, M., Wagner, E. F., Nishina, H., and Penninger, J. M. (2004) MKK7 couples stress signaling to G_2/M cell cycle progression and cellular senescence. *Nat. Cell Biol.* **6,** 215–226
8. Dunlap, J. C. (1999) Molecular bases for circadian clocks. *Cell* **96,** 271–290
9. King, D. P., and Takahashi, J. S. (2000) Molecular genetics of circadian rhythms in mammals. *Annu. Rev. Neurosci.* **23,** 713–742
10. Schibler, U., and Sassone-Corsi, P. (2002) A web of circadian pacemakers. *Cell* **111,** 919–922
11. Reppert, S. M., and Weaver, D. R. (2002) Coordination of circadian timing in mammals. *Nature* **418,** 935–941
12. Hirayama, J., and Sassone-Corsi, P. (2005) Structural and functional features of transcription factors controlling the circadian clock. *Curr. Opin. Genet. Dev.* **15,** 548–556
13. Gallego, M., and Virshup, D. M. (2007) Post-translational modifications regulate the ticking of the circadian clock. *Nat. Rev. Mol. Cell Biol.* **8,** 139–148
14. Uchida, Y., Hirayama, J., and Nishina, H. (2010) A common origin. Signaling similarities in the regulation of the circadian clock and DNA damage responses. *Biol. Pharm. Bull.* **33,** 535–544
15. Lowrey, P. L., Shimomura, K., Antoch, M. P., Yamazaki, S., Zemenides, P. D., Ralph, M. R., Menaker, M., and Takahashi, J. S. (2000) Positional syntenic cloning and functional characterization of the mammalian circadian mutation tau. *Science* **288,** 483–492
16. Toh, K. L., Jones, C. R., He, Y., Eide, E. J., Hinz, W. A., Virshup, D. M., Ptácek, L. J., and Fu, Y. H. (2001) An hPer2 phosphorylation site mutation in familial advanced sleep phase syndrome. *Science* **291,** 1040–1043
17. Akashi, M., Tsuchiya, Y., Yoshino, T., and Nishida, E. (2002) Control of intracellular dynamics of mammalian period proteins by casein kinase I ε (CKIε) and CKIδ in cultured cells. *Mol. Cell Biol.* **22,** 1693–1703
18. Eide, E. J., Woolf, M. F., Kang, H., Woolf, P., Hurst, W., Camacho, F., Vielhaber, E. L., Giovanni, A., and Virshup, D. M. (2005) Control of mammalian circadian rhythm by CKIε-regulated proteasome-mediated PER2 degradation. *Mol. Cell Biol.* **25,** 2795–2807
19. Vanselow, K., Vanselow, J. T., Westermark, P. O., Reischl, S., Maier, B., Korte, T., Herrmann, A., Herzel, H., Schlosser, A., and Kramer, A. (2006) Differential effects of PER2 phosphorylation. Molecular basis for the human familial advanced sleep phase syndrome (FASPS). *Genes Dev.* **20,** 2660–2672
20. Xu, Y., Toh, K. L., Jones, C. R., Shin, J. Y., Fu, Y. H., and Ptácek, L. J. (2007) Modeling of a human circadian mutation yields insights into clock regulation by PER2. *Cell* **128,** 59–70
21. Rennefahrt, U. E., Illert, B., Kerkhoff, E., Troppmair, J., and Rapp, U. R. (2002) Constitutive JNK activation in NIH 3T3 fibroblasts induces a partially transformed phenotype. *J. Biol. Chem.* **277,** 29510–29518
22. Hirayama, J., Sahar, S., Grimaldi, B., Tamaru, T., Takamatsu, K., Nakahata, Y., and Sassone-Corsi, P. (2007) CLOCK-mediated acetylation of BMAL1 controls circadian function. *Nature* **450,** 1086–1090
23. Yagita, K., Tamanini, F., Yasuda, M., Hoeijmakers, J. H., van der Horst, G. T., and Okamura, H. (2002) Nucleocytoplasmic shuttling and mCRY-dependent inhibition of ubiquitylation of the mPER2 clock protein. *EMBO J.* **21,** 1301–1314
24. Tsuchiya, Y., and Nishida, E. (2003) Mammalian cultured cells as a model system of peripheral circadian clocks. *J. Biochem.* **134,** 785–790
25. Schramek, D., Kotsinas, A., Meixner, A., Wada, T., Elling, U., Pospisilik, J. A., Neely, G. G., Zwick, R. H., Sigl, V., Forni, G., Serrano, M., Gorgoulis, V. G., and Penninger, J. M. (2011) The stress kinase MKK7 couples oncogenic stress to p53 stability and tumor suppression. *Nat. Genet.* **43,** 212–219
26. Yamasaki, T., Kawasaki, H., Arakawa, S., Shimizu, K., Shimizu, S., Reiner, O., Okano, H., Nishina, S., Azuma, N., Penninger, J. M., Katada, T., and Nishina, H. (2011) Stress-activated protein kinase MKK7 regulates axon elongation in the developing cerebral cortex. *J. Neurosci.* **31,** 16872–16883
27. Yagita, K., Yamanaka, I., Koinuma, S., Shigeyoshi, Y., and Uchiyama, Y. (2009) Mini screening of kinase inhibitors affecting period-length of mammalian cellular circadian clock. *Acta Histochem. Cytochem.* **42,** 89–93
28. Gdalyahu, A., Ghosh, I., Levy, T., Sapir, T., Sapoznik, S., Fishler, Y., Azoulai, D., and Reiner, O. (2004) DCX, a new mediator of the JNK pathway. *EMBO J.* **23,** 823–832
29. Nishitai, G., Shimizu, N., Negishi, T., Kishimoto, H., Nakagawa, K., Kitagawa, D., Watanabe, T., Momose, H., Ohata, S., Tanemura, S., Asaka, S., Kubota, J., Saito, R., Yoshida, H., Mak, T. W., Wada, T., Penninger, J. M., Azuma, N., Nishina, H., and Katada, T. (2004) Stress induces mitochondria-mediated apoptosis independent of SAPK/JNK activation in embryonic stem cells. *J. Biol. Chem.* **279,** 1621–1626
30. Yagita, K., Horie, K., Koinuma, S., Nakamura, W., Yamanaka, I., Urasaki, A., Shigeyoshi, Y., Kawakami, K., Shimada, S., Takeda, J., and Uchiyama, Y. (2010) Development of the circadian oscillator during differentiation of mouse embryonic stem cells *in vitro*. *Proc. Natl. Acad. Sci. U.S.A.* **107,** 3846–3851
31. Zhang, E. E., Liu, A. C., Hirota, T., Miraglia, L. J., Welch, G., Pongsawakul,

P. Y., Liu, X., Atwood, A., Huss, J. W., 3rd, Janes, J., Su, A. I., Hogenesch, J. B., and Kay, S. A. (2009) A genome-wide RNAi screen for modifiers of the circadian clock in human cells. *Cell* **139,** 199–210
32. Tanemura, S., Momose, H., Shimizu, N., Kitagawa, D., Seo, J., Yamasaki, T., Nakagawa, K., Kajiho, H., Penninger, J. M., Katada, T., and Nishina, H. (2009) Blockage by SP600125 of Fcϵ receptor-induced degranulation and cytokine gene expression in mast cells is mediated through inhibition of phosphatidylinositol 3-kinase signaling pathway. *J. Biochem.* **145,** 345–354
33. Kim, J. A., Lee, J., Margolis, R. L., and Fotedar, R. (2010) SP600125 suppresses Cdk1 and induces endoreplication directly from G2 phase, independent of JNK inhibition. *Oncogene* **29,** 1702–1716
34. Fu, L., Pelicano, H., Liu, J., Huang, P., and Lee, C. (2002) The circadian gene Period2 plays an important role in tumor suppression and DNA damage response *in vivo*. *Cell* **111,** 41–50
35. Oklejewicz, M., Destici, E., Tamanini, F., Hut, R. A., Janssens, R., and van der Horst, G. T. (2008) Phase resetting of the mammalian circadian clock by DNA damage. *Curr. Biol.* **18,** 286–291
36. Tsuchiya, Y., Akashi, M., Matsuda, M., Goto, K., Miyata, Y., Node, K., and Nishida, E. (2009) Involvement of the protein kinase CK2 in the regulation of mammalian circadian rhythms. *Sci. Signal.* **2,** ra26
37. Maier, B., Wendt, S., Vanselow, J. T., Wallach, T., Reischl, S., Oehmke, S., Schlosser, A., and Kramer, A. (2009) A large-scale functional RNAi screen reveals a role for CK2 in the mammalian circadian clock. *Genes Dev.* **23,** 708–718
38. Reischl, S., Vanselow, K., Westermark, P. O., Thierfelder, N., Maier, B., Herzel, H., and Kramer, A. (2007) β-TrCP1-mediated degradation of PERIOD2 is essential for circadian dynamics. *J. Biol. Rhythms* **22,** 375–386
39. Takano, A., Shimizu, K., Kani, S., Buijs, R. M., Okada, M., and Nagai, K. (2000) Cloning and characterization of rat casein kinase 1ϵ. *FEBS Lett.* **477,** 106–112
40. Vielhaber, E., Eide, E., Rivers, A., Gao, Z. H., and Virshup, D. M. (2000) Nuclear entry of the circadian regulator mPER1 is controlled by mammalian casein kinase I ϵ. *Mol. Cell Biol.* **20,** 4888–4899
41. Eide, E. J., Vielhaber, E. L., Hinz, W. A., and Virshup, D. M. (2002) The circadian regulatory proteins BMAL1 and cryptochromes are substrates of casein kinase Iϵ. *J. Biol. Chem.* **277,** 17248–17254
42. Kondratov, R. V., Kondratova, A. A., Gorbacheva, V. Y., Vykhovanets, O. V., and Antoch, M. P. (2006) Early aging and age-related pathologies in mice deficient in BMAL1, the core componentof the circadian clock. *Genes Dev.* **20,** 1868–1873
43. Nakamura, Y., Harama, D., Shimokawa, N., Hara, M., Suzuki, R., Tahara, Y., Ishimaru, K., Katoh, R., Okumura, K., Ogawa, H., Shibata, S., and Nakao, A. (2011) Circadian clock gene Period2 regulates a time-of-day-dependent variation in cutaneous anaphylactic reaction. *J. Allergy Clin. Immunol.* **127,** 1038–1045
44. Shimba, S., Ishii, N., Ohta, Y., Ohno, T., Watabe, Y., Hayashi, M., Wada, T., Aoyagi, T., and Tezuka, M. (2005) Brain and muscle Arnt-like protein-1 (BMAL1), a component of the molecular clock, regulates adipogenesis. *Proc. Natl. Acad. Sci. U.S.A.* **102,** 12071–12076
45. Grimaldi, B., Bellet, M. M., Katada, S., Astarita, G., Hirayama, J., Amin, R. H., Granneman, J. G., Piomelli, D., Leff, T., and Sassone-Corsi, P. (2010) PER2 controls lipid metabolism by direct regulation of PPARγ. *Cell Metab.* **12,** 509–520
46. Marcheva, B., Ramsey, K. M., Buhr, E. D., Kobayashi, Y., Su, H., Ko, C. H., Ivanova, G., Omura, C., Mo, S., Vitaterna, M. H., Lopez, J. P., Philipson, L. H., Bradfield, C. A., Crosby, S. D., JeBailey, L., Wang, X., Takahashi, J. S., and Bass, J. (2010) Disruption of the clock components CLOCK and BMAL1 leads to hypoinsulinemia and diabetes. *Nature* **466,** 627–631

Appl Magn Reson (2012) 42:69–77
DOI 10.1007/s00723-011-0275-8

Applied
Magnetic Resonance

Light, Reactive Oxygen Species, and Magnetic Fields Activating ERK/MAPK Signaling Pathway in Cultured Zebrafish Cells

Yoshimi Uchida · Tadanori Shimomura · Jun Hirayama · Hiroshi Nishina

Received: 29 May 2011 / Revised: 22 August 2011 / Published online: 27 September 2011

Abstract To guarantee that organism's biological rhythms remain tied to the rhythms of its environment, the circadian clock must be able to reset itself in response to environmental cues. The main environmental stimulus for organisms is light, which is provided by day–night cycles. Cultured lines of zebrafish cells have been established as an attractive vertebrate cell-based model suitable for the examination of the light signaling pathway for entraining the circadian clock. Studies using these cell lines have revealed critical roles for the mitogen-activated protein kinase (MAPK) signaling pathways in light-dependent circadian entrainment. Here, we show in cultured zebrafish cells that artificial magnetic fields induce extracellular signal-regulated kinase (ERK)/MAPK activation with kinetics analogous to those elicited by light, suggesting that magnetic fields may influence circadian regulation in zebrafish. Our findings indicate that cultured zebrafish cells represent a valuable system for investigating the links between magnetic fields and the signaling pathways responsible for the synchronization of vertebrate circadian clocks under laboratory conditions.

1 Introduction

Circadian clocks are endogenous oscillators that drive the daily rhythms of organisms ranging from bacteria to humans [1]. These clocks regulate various biochemical, physiological, and behavioral processes with a periodicity of approximately 24 h [2]. Under natural conditions, circadian rhythms are entrained to this 24 h period by

Electronic supplementary material The online version of this article (doi:10.1007/s00723-011-0275-8) contains supplementary material, which is available to authorized users.

Y. Uchida · T. Shimomura · J. Hirayama (✉) · H. Nishina
Department of Developmental and Regenerative Biology, Medical Research Institute, Tokyo Medical and Dental University, 1-5-45 Yushima, Bunkyo-ku, Tokyo 113-8510, Japan
e-mail: hirayama.dbio@mri.tmd.ac.jp

environmental time cues, light levels being the most important. The core of the clock mechanism in almost all organisms studied to date is a transcription/translation-based negative feedback loop that relies on positive and negative oscillators [3, 4]. In vertebrates, three basic helix–loop–helix Per-ARNT-Sim (PAS) domain-containing transcription factors, called CLOCK, NPAS2 and BMAL, constitute the positive elements. CLOCK or NPAS2 heterodimerizes with BMAL to form a transcriptionally active complex that binds to E-box elements (CACGTG) present in the promoters of members of the *Period* (*Per*) and *Cryptochrome* (*Cry*) gene families. Once the PER and CRY proteins have been translated, they form heterodimers that can then translocate to the nucleus to repress CLOCK (NPAS2):BMAL-mediated transcription through direct protein–protein interaction. These interactions then set up the rhythmic oscillations of gene expression that drive the circadian clock.

Zebrafish has been established as an attractive vertebrate model suitable for the examination of the light signaling pathway and its impact on the circadian clock [5, 6]. Not only are the molecular components of the mammalian and zebrafish circadian oscillators highly similar, but also zebrafish clocks have the unusual attribute of being directly light responsive. In zebrafish organs, tissues and cultured cells, exposure to an acute light pulse leads to the transactivation of two clock genes, *zCry1a* and *zPer2*, and entrains oscillations of clock gene expression to a new light–dark cycle [7–9]. Importantly, studies in zebrafish have revealed critical roles for the cellular redox state and mitogen-activated protein kinase (MAPK) signaling pathways in the regulation of light-dependent gene expression [10, 11]. In a variety of organisms, light induces reactive oxygen species (ROS) production that alters the redox state within cells [12]. In zebrafish cells, a light-induced change in redox state stimulates extracellular signal-regulated kinase (ERK)/MAPK signaling, which in turn transduces photic signals to *zCry1a* and *zPer2* transcription [9, 11, 13]. When *zCry1a* and *zPer2* expression is induced by such signals, zCRY1a and zPER2 proteins can initiate the light-dependent entrainment process in zebrafish cells kept permanently in the dark.

Magnetic fields have been shown to influence the circadian clock in invertebrate and vertebrate species [14, 15]. Interestingly, more recent studies have reported that CRY works as a magnetosensor in birds and *Drosophila* [16–18]. The underlying molecular mechanisms of how magnetic fields impact on circadian clocks are, however, unclear.

In this study, we found that magnetic fields increase ERK phosphorylation in zebrafish cells and that this profile is analogous to that of light-dependent ERK activation. Because ERK activation is an essential step for the light-dependent circadian regulation [10, 11], our results indicate that magnetic fields may regulate the zebrafish circadian clock and further that cultured zebrafish cells are indeed a valid model system for the analysis of vertebrate circadian clocks.

2 Materials and Methods

2.1 Reagents and Antibodies

Anti-ERK and anti-phospho-ERK primary antibodies were purchased from Cell Signaling and New England Biolab, respectively. Anti-JNK and anti-phospho-JNK

primary antibodies were purchased from Santa Cruz Biotechnology and Cell Signaling, respectively.

2.2 Cell Culture, Enzyme Inhibition and Light Induction

Cultured zebrafish cells were prepared as described previously [19] and maintained at 28°C in L-15 medium (Sigma–Aldrich) containing 10% fetal bovine serum. Cultured dishes were kept in a water-jacketed, thermostatically controlled, and light-sealed incubator (SANYO MIR-154). Illumination was achieved by using a fluorescent light source equipped within the incubator. The intensity of light in the present study was approximately 500 lux. This intensity has been reported to be sufficient for entrainment of circadian gene expression in zebrafish cells [20].

2.3 Immunoblotting

Cells were homogenized in a binding buffer (150 mM NaCl, 1 mM ethylenediaminetetraacetic acid, 0.5% Nonidet P-40, 1 mM ethyleneglycoltetraacetic acid, 5% glycerol, and 20 mM Tris–HCl, pH 7.4), containing protease inhibitor mixture tablets. Lysates were fractionated by SDS-PAGE and transferred by electroblotting onto polyvinylidene difluoride membranes. Membranes were blocked with 2 or 5% nonfat milk and incubated for 10 h at 4°C with primary anti-total ERK or anti-phospho-ERK antibody. Blots were then incubated with the appropriate secondary antibody and developed with the ECL Western blotting detection system (Amersham Biosciences).

2.4 Magnetic Fields

Magnetic fields were produced by a permanent magnet. The intensity of the magnetic fields was measured with a tesla meter (KANETEC TM-701). Zebrafish cells were cultured in 3.5 cm dishes (Iwaki). The culture dishes were placed on the square magnets (4.5 × 3.7 × 0.6 cm) in such a way that the magnetic poles horizontally faced each other on either side of the culture dish. For the treatment of magnetic fields, we prepared a dark room, where the temperature was set at 28°C. Because zebrafish cultured cells grow in atmospheric CO_2, we did not maintain them in incubator so that their functions were not affected. Untreated control cells were maintained in separate (but otherwise identical) place of the dark room, so that the magnetic fields would not affect the control cells. Finally, we did all the handling in the dark.

3 Results

3.1 Light Inducing Oscillatory Activation of ERK

We first examined the effects of light on ERK/MAPK phosphorylation in cultured zebrafish cells. Cells were kept in the dark prior to exposure to light, then harvested at various time points from 0 to 120 min after light stimulation, and protein extracts

were immunoblotted to detect total and phospho-ERK levels. Consistent with our previous report [11], phospho-ERK levels increased significantly at 5 min after light exposure (Fig. 1a). Importantly, we confirmed that phospho-ERK levels were constant in cultured zebrafish cells kept in the dark without any stimuli (Fig. S1).

We next examined the profile of ERK/MAPK phosphorylation in cultured zebrafish cells exposed to 12 h light–12 h dark (LD) cycle. Cells were kept in the dark prior to exposure to light, harvested every 2 h after light stimulation, and protein extracts were immunoblotted to detect total and phospho-ERK levels. Interestingly, we found that ERK phosphorylation, and therefore activity, oscillated in response to light stimulation in zebrafish cultured cells (Fig. 1b).

3.2 H_2O_2 Activating ERK/MAPK Signaling in Zebrafish Cells

ROS are well-established second messengers involved in redox signaling that have been recently identified as key signaling mediators in zebrafish circadian transcription [9, 12, 13]. We have previously provided evidence that ERK/MAPK signaling mediates ROS-dependent circadian transcription in cultured zebrafish cells [9]. However, the direct effect of ROS on ERK phosphorylation in zebrafish cultured cells has not been examined. We therefore analyzed the effect of H_2O_2, a well-known ROS, on ERK phosphorylation levels in zebrafish cells. Cultured

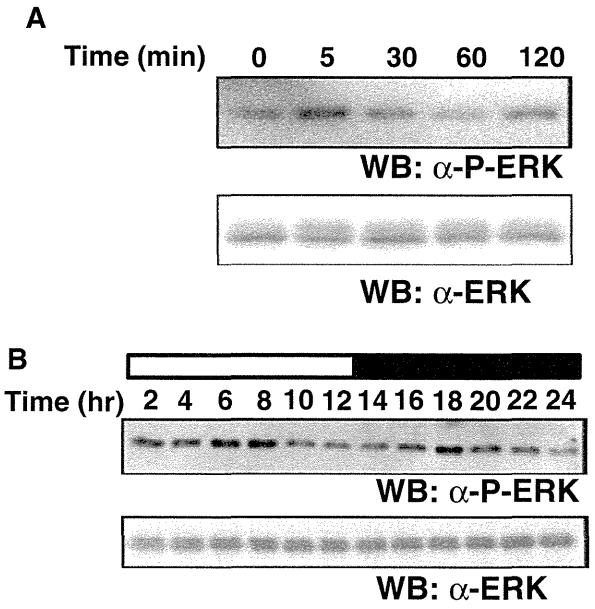

Fig. 1 Light induces oscillatory activation of ERK in cultured zebrafish cells. **a** Cultured zebrafish cells were maintained in constant darkness for 2 days. Cells were then exposed to light for the indicated times and protein extracts were immunoblotted to detect phospho-ERK (P-ERK) and total ERK. Results shown are representative of three independent experiments. **b** Cultured zebrafish cells were maintained in constant darkness for 2 days. Cells were then exposed to light for 12 h. Protein extracts at the indicated times were immunoblotted to detect phospho-ERK (P-ERK) and total ERK. Results shown are representative of three independent experiments. The *bar* above the blots indicates light (*white*) and dark (*black*) periods

zebrafish cells were kept in the dark prior to H_2O_2 treatment. Cells were then harvested at various time points from after the start of the H_2O_2 treatment, and extracts were immunoblotted to detect total and phospho-ERKs. As shown in Fig. 2, phospho-ERK levels increased significantly at 5 min after start of the H_2O_2 treatment. Importantly, the profile of H_2O_2-induced phosphorylation of ERK is analogous to that of light-dependent ERK activation. These findings are consistent with the idea that ROS are second messengers activating the ERK/MAPK signaling pathway to regulate circadian transcription.

3.3 Magnetic Fields Inducing ERK Phosphorylation

It has been previously reported that magnetic fields increase intracellular ROS levels in cultured cells [21]. In addition, our data showed that treatment of zebrafish cultured cells with H_2O_2 induced ERK phosphorylation (Fig. 2). We therefore speculated that magnetic fields may induce ERK phosphorylation in zebrafish cultured cells. To test this possibility, we examined the effects of magnetic fields on ERK/MAPK activation. Cultured zebrafish cells were treated with magnetic fields in the dark. Cells were harvested at various time points from 0 to 120 min after the treatment, and extracts were immunoblotted to detect total and phospho-ERKs. Interestingly, phospho-ERK levels increased significantly at 5 min after treatment with magnetic fields (Fig. 3a). We also examined the effects of magnetic fields on the c-Jun N-terminal kinase (JNK) signaling pathway. We found that phosphorylation levels of JNK increased significantly at 5 min after treatment with magnetic fields (Fig. 3b). In contrast, phospho-JNK levels were constant in cultured zebrafish cells kept in darkness without any stimuli (Fig. S2). Notably, the magnetic field stimulus used in the present study is $\sim$1,000,000 times stronger than the regular daily variation in the magnetic field, which has been proposed to serve as a zeitgeber for the circadian clock [22, 23]. Thus, we would like to stress that the strong magnetic fields we used can have qualitatively different effects on biological molecules than earth-strength magnetic fields.

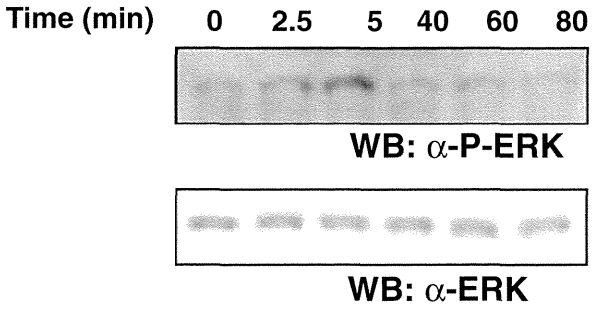

Fig. 2 H_2O_2 induces ERK phosphorylation in zebrafish cells. Cultured zebrafish cells were maintained in constant darkness for 2 days. Cells were then treated with H_2O_2 (10 μM) for the indicated times and protein extracts were immunoblotted to detect phospho-ERK (P-ERK) and total ERK. Results shown are representative of three independent experiments

4 Discussion

In many organisms, external stimuli are connected to a cell's nucleus via signal transduction mechanisms, with the MAPK pathway being a prominent signaling player. Moreover, the role for MAPKs in circadian clock regulation has been well established [2, 24, 25]. There are three major MAPKs: JNK, p38, and ERK. We have previously reported in cultured zebrafish cells that the phosphorylation level of ERK is induced by light, peaking 5 min after the light onset, and that the acute light induction of ERK activation is essential for light-dependent circadian clock regulation [11]. To better characterize the response of ERK activation to light, our current study examined the profile of ERK phosphorylation in cultured zebrafish cells exposed to the LD cycle. Interestingly, ERK phosphorylation oscillated in light-treated cells (Fig. 1). The oscillation pattern of the ERK phosphorylation seemed to be biphasic. It is conceivable that the first peak during the light phase may be induced by light and the second peak during the night phase may be dependent on circadian machinery. It has been demonstrated that the growth factor stimulation induces oscillation of ERK activation in cultured mammalian cells [26]. Thus, the oscillatory activation of ERK seems to be a conserved biological event among vertebrates, although its physiological significance still needs to be investigated.

ROS were originally thought to act solely as toxic metabolites due to their high reactivity with cell components such as deoxyribonucleic acid (DNA), proteins, and lipids to exert oxidative stress [12, 27]. However, ROS are also ideally suited to be signaling molecules because they are small in size and can easily diffuse short distances within a cell. In addition, mechanisms for ROS production by flavin-containing oxidases, as well as means for their rapid removal by catalases are

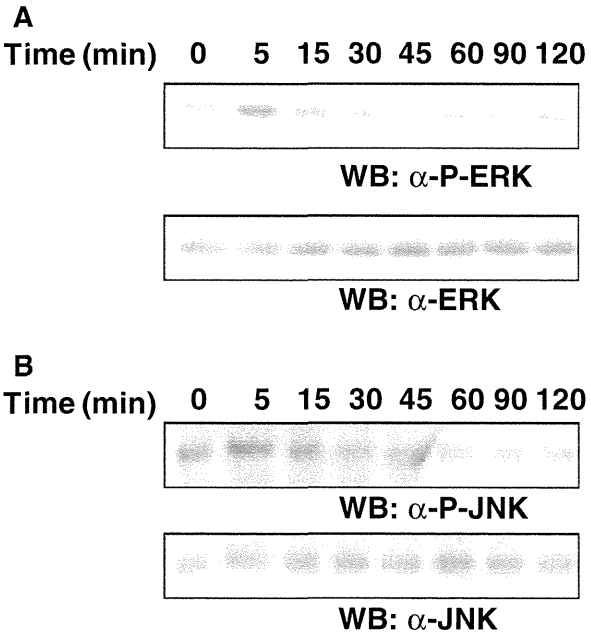

Fig. 3 Magnetic fields induce ERK phosphorylation in zebrafish cells. Cultured zebrafish cells were maintained in constant darkness for 2 days. Cells were then exposed to magnetic fields (30–70 mT) for the indicated times and protein extracts were immunoblotted to detect phospho-ERK (P-ERK) and total ERK (**a**) or phospho-JNK (P-JNK) and total JNK (**b**). Results shown are representative of three independent experiments

present in almost all cell types. In a variety of organisms, light induces ROS production leading to altered redox status [12, 28]. In zebrafish cells, this light-induced redox change increases the expression level of the *zCry1a* and *zPer2* genes, which are important players of the circadian clock [9, 13]. Our previous work revealed that the ERK/MAPK signaling pathway couples the light-induced ROS production to the entrainment of the circadian clock. Indeed, an inhibitor of ERK/MAPK signaling pathway, U0126, is capable of significantly inhibiting H_2O_2-induced expression of the *zCry1a* and *zPer2* genes [9]. In support of this idea, we found that H_2O_2 increases ERK phosphorylation with kinetics analogous to that of light-dependent ERK activation.

Previous studies have reported that magnetic fields activate MAPK signaling pathways [29, 30]. Interestingly, we found that magnetic fields activate ERK phosphorylation in cultured zebrafish cells. Because magnetic fields have been shown to increase intracellular ROS levels in cultured cells [21], it is conceivable that magnetic field-induced ERK activation in our system may be mediated by magnetic field-mediated ROS production. Furthermore, ERK activation by magnetic fields raises an important prospect, as it suggests that circadian transcription in zebrafish cells may be influenced by magnetic fields. Because the light-stimulated ERK/MAPK signaling pathway induces *zCry1a* and *zPer2* gene expression [10, 11], the ERK/MAPK signaling pathway activated by magnetic fields might also regulate the expression of these circadian genes. Whether magnetic fields contribute to signaling pathways regulating circadian clocks in zebrafish still needs to be addressed.

Recent studies have provided evidence for the involvement of CRYs in magnetoreception [17, 18]. However, activation of ERK/MAPK induced by magnetic fields in the present study (Fig. 3) seems to be mediated by a CRY-independent mechanism that is different from the mechanism proposed to play a role in sensing the geomagnetic field and, indeed, one that is unlikely to be involved in a directional sense ("compass") or in detecting the extremely weak ($\sim$50 nT) daily variation. In fact, the proposed effects of the geomagnetic fields on CRY-based magnetoreception mechanisms involve 'low-field' effects, which are typically in the range of 0.1–1 mT [22, 23]. In addition, the magnetic field stimulus used in our study is $\sim$1,000,000 times stronger than the regular daily variation in the magnetic field, which has been proposed to serve as a zeitgeber for the circadian clock [22, 23]. Thus, it should be stressed that the strong magnetic fields in the present study can have qualitatively different effects on biological molecules than earth-strength magnetic fields.

The strong magnetic fields have been shown to influence a variety of cellular regulatory steps. In fact, they can affect transcription of various genes such as *interleukin-6* and *bone sialoprotein* [31, 32], posttranslational modification of proteins [29, 30], DNA binding activity of transcription factors [32, 33], and cellular reduction–oxidation state [21, 34]. Notably, these regulatory elements have critical roles to establish and maintain many biological systems including the circadian clock and cell cycle. Thus, it is conceivable that the strong magnetic fields can have multiple effects on these biological systems. In support of this idea, the magnetic fields have been shown to affect the growth of neuronal and muscle cells [35, 36], and they also modulate differentiation of human osteoblasts and embryonic cells [31, 37].

Vertebrate circadian feedback loops in peripheral cells are affected by an enormous variety of non-photic stimuli known to induce intracellular signaling pathways, including those involving protein kinase C, glucocorticoid, Wnt, tumor growth factor-b/activin, and MAPKs [5, 38, 39]. Thus, it is likely that a variety of different signaling cascades are involved in entrainment of peripheral clocks. However, the mechanisms by which these signaling pathways, alone or in combination with the other pathways, synchronize peripheral circadian feedback loops, as well as the physiological role of the non-photic entrainment, are still poorly understood [5]. Our finding of ERK/MAPK activation by the strong magnetic fields indicates that these may be a useful tool for producing non-photic entrainment of the circadian clocks under laboratory conditions. The studies using the strong magnetic fields as a resetting cue for the circadian clocks may allow more thorough investigations of the signaling cascades involved in entraining and maintaining circadian feedback loops and may give insight into how such signaling mechanisms have evolved.

Acknowledgments We are grateful to all members of the Nishina Laboratory for their insightful comments. This work was supported by a Grant-in-Aid for Scientific Research on a Priority Area from the Ministry of Education, Culture, Sport, Science and Technology of Japan, and the Ministry of Health, Labor and Welfare of Japan.

References

1. D.P. King, J.S. Takahashi, Annu. Rev. Neurosci. **23**, 713–742 (2000)
2. J. Hirayama, P. Sassone-Corsi, Curr. Opin. Genet. Dev. **15**, 548–556 (2005)
3. J.C. Dunlap, Cell **96**, 271–290 (1999)
4. S.M. Reppert, D.R. Weaver, Nature **418**, 935–941 (2002)
5. Y. Uchida, J. Hirayama, H. Nishina, Biol. Pharm. Bull. **33**, 535–544 (2010)
6. G. Vatine, D. Vallone, N.Y. Gothilf, S. Foulkes, FEBS Lett. **585**, 1485–1494 (2011)
7. L. Ziv, S. Levkovitz, R. Toyama, J. Falcon, Y. Gothilf, J. Neuroendocrinol. **17**, 314–320 (2005)
8. T.K. Tamai, L.C. Young, D. Whitmore, Proc. Natl. Acad. Sci. USA **104**, 14712–14717 (2007)
9. J. Hirayama, S. Cho, P. Sassone-Corsi, Proc. Natl. Acad. Sci. USA **104**, 15747–15752 (2007)
10. N. Cermakian, M.P. Pando, C.L. Thompson, A.B. Pinchak, C.P. Selby, L. Gutierrez, D.E. Wells, G.M. Cahill, A. Sancar, P. Sassone-Corsi, Curr. Biol. **12**, 844–848 (2002)
11. J. Hirayama, N. Miyamura, Y. Uchida, Y. Asaoka, R. Honda, K. Sawanobori, T. Todo, T. Yamamoto, P. Sassone-Corsi, H. Nishina, Cell Cycle **8**, 2794–2801 (2009)
12. S. Neill, R. Desikan, J. Hancock, Curr. Opin. Plant Biol. **5**, 388–395 (2002)
13. T. Osaki, Y. Uchida, J. Hirayama, H. Nishina, Biol. Pharm. Bull. **34**, 1343–1347 (2011)
14. H.B. Dowse, J.D. Palmer, Nature **222**, 564–566 (1969)
15. V.L. Bliss, F.H. Heppner, Nature **261**, 411–412 (1976)
16. H. Mouritsen, U. Janssen-Bienhold, M. Liedvogel, G. Feenders, J. Stalleicken, P. Dirks, R. Weiler, Proc. Natl. Acad. Sci. USA **101**, 14294–14299 (2004)
17. R.J. Gegear, A. Casselman, S. Waddell, S.M. Reppert, Nature **454**, 1014–1018 (2008)
18. T. Yoshii, M. Ahmad, C. Helfrich-Forster, PLoS Biol. **7**, e1000086 (2009)
19. M.P. Pando, A.B. Pinchak, N. Cermakian, P. Sassone-Corsi, Proc. Natl. Acad. Sci. USA **98**, 10178–10183 (2001)
20. D. Whitmore, N.S. Foulkes, P. Sassone-Corsi, Nature **404**, 87–91 (2000)
21. M. De Nicola, S. Cordisco, C. Cerella, M.C. Albertini, M. D'Alessio, A. Accorsi, A. Bergamaschi, A. Magrini, L. Ghibelli, Ann. N. Y. Acad. Sci. **1090**, 59–68 (2006)
22. C.T. Rodgers, P.J. Hore, Proc. Natl. Acad. Sci. USA **106**, 353–360 (2009)

23. I.A. Solov'yov, H. Mouritsen, K. Schulten, Biophys. J. **99**, 40–49 (2011)
24. G.M. Thomas, R.L. Huganir, Nat. Rev. Neurosci. **5**, 173–183 (2004)
25. M. Gallego, D.M. Virshup, Nat. Rev. Mol. Cell Biol. **8**, 139–148 (2007)
26. K. Nakayama, T. Satoh, A. Igari, R. Kageyama, E. Nishida, Curr. Biol. **18**, R332–R334 (2008)
27. S.J. Neill, R. Desikan, A. Clarke, R.D. Hurst, J.T. Hancock, J. Exp. Bot. **53**, 1237–1247 (2002)
28. P.E. Hockberger, T.A. Skimina, V.E. Centonze, C. Lavin, S. Chu, S. Dadras, J.K. Reddy, J.G. White, Proc. Natl. Acad. Sci. USA **96**, 6255–6260 (1999)
29. D. Malagoli, M. Lusvardi, F. Gobba, E. Ottaviani, Comp. Biochem. Physiol. C: Toxicol. Pharmacol. **137**, 75–79 (2004)
30. A. Prina-Mello, E. Farrell, P.J. Prendergast, V. Campbell, J.M. Coey, Bioelectromagnetics **27**, 35–42 (2006)
31. Z. Wang, A. Sarje, P.L. CheK, J. Yarema, BMC Genomics **10**, 356 (2009)
32. E. Shimizu, Y. Matsuda-Honjyo, H. Samoto, R. Saito, Y. Nakajima, Y. Nakayama, N. Kato, M. Yamazaki, Y. Ogata, J. Cell. Biochem. **91**, 1183–1196 (2004)
33. J. Zhou, G. Yao, J. Zhang, Z. Chang, Biochem. Biophys. Res. Commun. **296**, 1013–1018 (2002)
34. H. Okano, Front. Biosci. **13**, 6106–6125 (2008)
35. T.J. Kilpatrick, P.F. Bartlett, Neuron **10**, 255–265 (1993)
36. S. Kim, W. Im, Cell Biochem. Biophys. **57**, 1–8 (2010)
37. L. Yuge, A. Okubo, T. Miyashita, T. Kumagai, T. Nikawa, S. Takeda, M. Kanno, Y. Urabe, M. Sugiyama, K. Kataoka, Biochem. Biophys. Res. Commun. **311**, 32–38 (2003)
38. A. Balsalobre, L. Marcacci, U. Schibler, Curr. Biol. **10**, 1291–1294 (2000)
39. N. Kon, T. Hirota, T. Kawamoto, Y. Kato, T. Tsubota, Y. Fukada, Nat. Cell Biol. **10**, 1463–1469 (2008)

Cancer susceptibility and embryonic lethality in *Mob1a/1b* double-mutant mice

Miki Nishio,[1] Koichi Hamada,[1] Kohichi Kawahara,[1] Masato Sasaki,[2,3] Fumihito Noguchi,[4] Shuhei Chiba,[5] Kensaku Mizuno,[5] Satoshi O. Suzuki,[6] Youyi Dong,[7] Masaaki Tokuda,[7] Takumi Morikawa,[1] Hiroki Hikasa,[1] Jonathan Eggenschwiler,[8] Norikazu Yabuta,[9] Hiroshi Nojima,[9] Kentaro Nakagawa,[10] Yutaka Hata,[10] Hiroshi Nishina,[11] Koshi Mimori,[12] Masaki Mori,[12,13] Takehiko Sasaki,[2,14] Tak W. Mak,[3] Toru Nakano,[15] Satoshi Itami,[4] and Akira Suzuki[1,2]

[1]Division of Cancer Genetics, Medical Institute of Bioregulation, Graduate School of Medical Sciences, Kyushu University, Fukuoka, Japan. [2]Global Centers of Excellence Program, Akita University Graduate School of Medicine, Akita, Japan. [3]The Campbell Family Institute for Cancer Research, University Health Network, Toronto, Ontario, Canada. [4]Department of Regenerative Dermatology, Graduate School of Medicine, Osaka University, Suita, Osaka, Japan. [5]Department of Biomolecular Sciences, Graduate School of Life Sciences, Tohoku University, Sendai, Miyagi, Japan. [6]Department of Neuropathology, Graduate School of Medical Sciences, Kyushu University, Fukuoka, Japan. [7]Department of Cell Physiology, Faculty of Medicine, Kagawa University, Miki-cho, Kagawa, Japan. [8]Department of Molecular Biology, Princeton University, Princeton, New Jersey, USA. [9]Department of Molecular Genetics, Research Institute for Microbial Diseases, Osaka University, Suita, Osaka, Japan. [10]Department of Medical Biochemistry and [11]Department of Developmental and Regenerative Biology, Graduate School of Medicine, Tokyo Medical and Dental University, Tokyo, Japan. [12]Department of Surgery, Kyushu University, Beppu Hospital, Beppu, Oita, Japan. [13]Department of Gastroenterological Surgery, Graduate School of Medicine, Osaka University, Suita, Osaka, Japan. [14]Department of Medical Biology, Akita University Graduate School of Medicine, Akita, Japan. [15]Department of Pathology, Medical School and Graduate School of Frontier Biosciences, Osaka University, Suita, Osaka, Japan.

Mps one binder 1a (MOB1A) and MOB1B are key components of the Hippo signaling pathway and are mutated or inactivated in many human cancers. Here we show that intact *Mob1a* or *Mob1b* is essential for murine embryogenesis and that loss of the remaining WT *Mob1* allele in $Mob1a^{\Delta/\Delta}1b^{tr/+}$ or $Mob1a^{\Delta/+}1b^{tr/tr}$ mice results in tumor development. Because most of these cancers resembled trichilemmal carcinomas, we generated double-mutant mice bearing tamoxifen-inducible, keratinocyte-specific homozygous-null mutations of *Mob1a* and *Mob1b* (*k*DKO mice). *k*DKO mice showed hyperplastic keratinocyte progenitors and defective keratinocyte terminal differentiation and soon died of malnutrition. *k*DKO keratinocytes exhibited hyperproliferation, apoptotic resistance, impaired contact inhibition, enhanced progenitor self renewal, and increased centrosomes. Examination of Hippo pathway signaling in *k*DKO keratinocytes revealed that loss of *Mob1a/b* altered the activities of the downstream Hippo mediators LATS and YAP1. Similarly, YAP1 was activated in some human trichilemmal carcinomas, and some of these also exhibited MOB1A/1B inactivation. Our results clearly demonstrate that MOB1A and MOB1B have overlapping functions in skin homeostasis, and exert their roles as tumor suppressors by regulating downstream elements of the Hippo pathway.

Introduction

Tissue homeostasis requires a balance of cell proliferation, apoptosis, and differentiation. During tissue development, progenitor cells divide for a limited number of times before exiting the cell cycle and undergoing terminal differentiation (1). When progenitor cells proliferate inappropriately and/or undergo abnormal differentiation, cancer can result (2).

Skin is a tissue that begins as a single-layered epithelium made up of keratinocytes that later stratify and differentiate into hair follicles (HFs) or interfollicular epidermis (IFE). Disruption of signals balancing growth and differentiation in keratinocytes can initiate skin cancers. The most common skin cancer is basal cell carcinoma (BCC), the nodular subtype of which originates from HFs. Trichilemmal carcinomas are also HF-derived skin cancers, but are much more rare and show characteristic abnormalities of outer hair root sheath differentiation (3). Although impairment of the Sonic Hedgehog (SHH) intracellular signaling pathway is now well established as the cause of BCC (4, 5), the molecular mechanism underlying the development of trichilemmal carcinomas is unknown.

The evolutionarily conserved Hippo signaling pathway was first identified as regulating the cell proliferation and apoptosis-controlling organ size in *Drosophila* (6, 7). In mammals, the canonical Hippo pathway includes the following: Neurofibromin 2 (NF2) (8), the Mammalian STE20-like protein (MST) kinases (9), large tumor suppressor homolog (LATS) and Nuclear Dbf2-related (NDR) kinases (10), the adaptor proteins SAV1 (WW45) (11) and MOB (12), and their downstream transcriptional coactivators YAP1 and its paralog transcriptional coactivator with PDZ-binding motif (TAZ, WWTR1) (13). All of these molecules (except YAP1 and TAZ) have been implicated as tumor suppressors. For example, mice deficient in *Lats1* or *Mst1/2* develop various cancers (14, 15), SAV1 and MOB are mutated in human cancer cell lines (16, 17), and Hippo components are reduced in human cancer samples (18). Homozygous-null mutant mice lacking *Nf2*, *Mst1/2*, *Sav1*, *Lats2*, or *Yap1* are all embryonic lethal (15, 19–22), precluding study of these mediators in tumorigenesis. To complicate matters, multiple homologs of each mammalian Hippo element exist, and a noncanonical Hippo pathway influences the localization and activity of canonical Hippo components (15, 23). Thus, the precise physiological functions of Hippo elements in mammals remain obscure.

Authorship note: Koichi Hamada and Kohichi Kawahara contributed equally to this work. Satoshi Itami and Akira Suzuki contributed equally as co-senior authors.

Conflict of interest: The authors have declared that no conflict of interest exists.

Citation for this article: *J Clin Invest.* 2012;122(12):4505–4518. doi:10.1172/JCI63735.

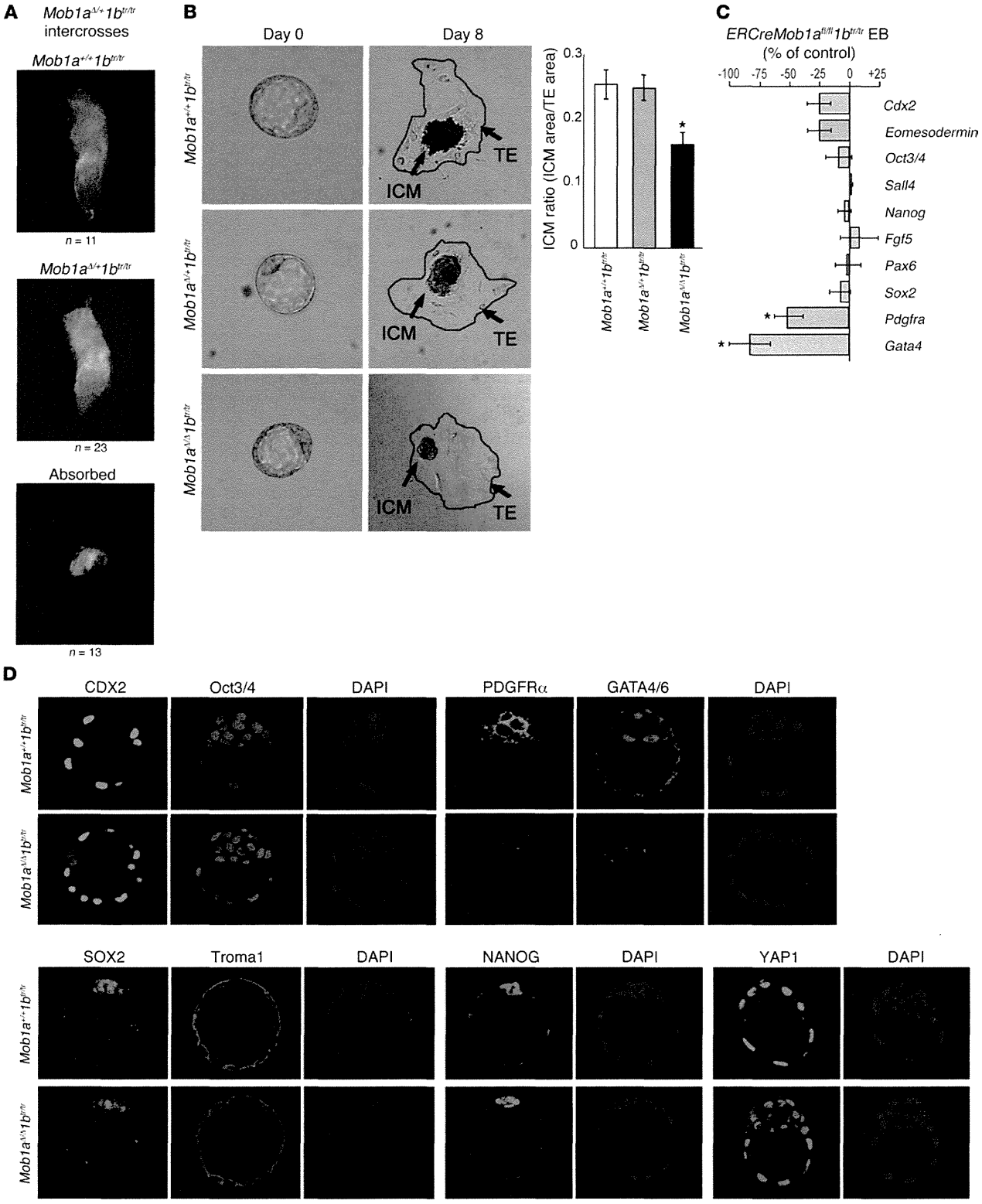
A
Mob1a+/+1btr/tr intercrosses
Mob1a+/+1btr/tr
n = 11
Mob1a+/-1btr/tr
n = 23
Absorbed
n = 13
B
Day 0
Day 8
Mob1a+/+1btr/tr
Mob1a+/-1btr/tr
Mob1a-/-1btr/tr
ICM
TE
ICM ratio (ICM area/TE area)
0.3
0.2
0.1
0
C
ERCreMob1aflfl1btr/tr EB
(% of control)
-100 -75 -50 -25 0 +25
Cdx2
Eomesodermin
Oct3/4
Sall4
Nanog
Fgf5
Pax6
Sox2
Pdgfra
Gata4
D
CDX2
Oct3/4
DAPI
PDGFRα
GATA4/6
DAPI
SOX2
Troma1
DAPI
NANOG
DAPI
YAP1
DAPI

Figure 1
Loss of *Mob1a/1b* impairs mouse embryo survival. (**A**) Morphologies of representative E6.5 embryos of the indicated genotypes from $Mob1a^{\Delta/+}1b^{tr/tr}$ intercrosses. $Mob1a^{\Delta/\Delta}1b^{tr/tr}$ embryos were absorbed after implantation. (**B**) Left: photographs of E3.5 blastocysts of the indicated genotypes on day 0 and after culture for 8 days. The ICM is surrounded by TE giant cells. Right: mean ICM ratio (ICM area/TE area) ± SEM plotted for blastocysts of the indicated genotypes (n = 8/group); $^*P < 0.01$. (**C**) Quantitative PCR determination of mRNAs for the indicated genes in EBs generated from $ERCreMob1a^{fl/fl}1b^{tr/tr}$ ES cells. ES cells were cultured with/without tamoxifen for 2 days, and control and mutant EBs were generated using the hanging drop method after culture for 3 days (*Cdx2*, *Eomesodermin*, *Oct3/4*, *Sall4*) or 4 days (*Nanog*, *Fgf5*, *Pax6*, *Sox2*, *Pdgfra*, *Gata4*). mRNA levels in the mutant are expressed as the percentage increase over control values; $^*P < 0.05$. (**D**) Immunostaining to detect the indicated proteins in blastocysts of the indicated genotypes. Nuclei were visualized with DAPI. Results shown are representative of at least 3 independent trials and at least 3 mice/group. Data are presented as the mean ± SEM, and P values were determined using the 2-tailed Student's t test.

MOB1 was originally shown in yeast to regulate mitotic exit and modulate cytokinesis (24–29). In *Drosophila*, *dMOB1* (*MATS*) overexpression is tumor suppressive, while loss of *dMOB1* triggers tumor development (17). In humans, 7 MOB homologs (hMOB1A-B, 2A-C, 3, 4, where MOB indicates Mps one binder) have been identified (30), and hMOB1A (hMATS1, MOBKL1B) and hMOB1B (hMATS2, MOBKL1A) share 95% amino acid identity. Although no apparent functional domain has been found in hMOB1A/1B, only these 2 MOB proteins can bind to and activate LATS1/2 (31). In vitro, hMOB1A overexpression inhibits cell proliferation, while suppression of hMOB1B or hMOB1A mediated by shRNA or siRNA increases proliferation (30) or impairs mitotic exit (32), respectively. In vivo, the *hMOB1A* gene is mutated in melanoma and breast cancer cell lines, and its expression is downregulated in human colorectal and non–small-cell lung cancers (17, 33, 34). However, the normal function of hMOB1 proteins in vivo is unknown. To assess whether MOB1 is an important functional component of mammalian Hippo signaling and to determine whether MOB1 is truly a tumor suppressor in vivo, we generated and characterized double-mutant mice lacking *Mob1a* and *Mob1b*.

Results

Embryonic lethality of Mob1a/1b-null mutant mice. We first generated single-mutant mice bearing a null mutation of *Mob1a* ($Mob1a^{\Delta/\Delta}$) or a trapped mutation of *Mob1b* ($Mob1b^{tr/tr}$) (Supplemental Figure 1, A–D; supplemental material available online with this article; doi:10.1172/JCI63735DS1) but no abnormalities were observed in morphology, body weight, histology, or life span (Supplemental Figure 1E and data not shown). We then attempted to generate double-homozygous–null mutant ($Mob1a^{\Delta/\Delta}1b^{tr/tr}$) mice, but no viable pups were obtained (Supplemental Table 1), indicating that complete loss of *Mob1* is embryonic lethal. We next analyzed embryos from $Mob1A^{\Delta/+}1b^{tr/tr}$ intercrosses at various time points during gestation. By E6.5, although decidua were formed, 28% of embryos were absorbed too severely to genotype (Figure 1A and Table 1). Thus, MOB1A and MOB1B have overlapping functions, and MOB1 is essential for postimplantation embryogenesis.

To pinpoint the embryonic defect, we obtained individual blastocysts (E3.5) from $Mob1a^{\Delta/+}1b^{tr/tr}$ intercrosses and cultured them for 8 days. $Mob1a^{\Delta/\Delta}1b^{tr/tr}$ blastocysts appeared normal at E3.5, but showed growth failure of the inner cell mass (ICM) by day 8 (Figure 1B). In contrast, the trophectoderm (TE) of $Mob1a^{\Delta/\Delta}1b^{tr/tr}$ blastocysts developed normally.

To create conditional tamoxifen-inducible *Mob1* mutants, we generated $ERCreMob1a^{fl/fl}1b^{tr/tr}$ ES cells and established embryoid bodies (EBs) using the hanging drop method. Control and mutant EBs were cultured for 2 days with (or without) tamoxifen to delete *Mob1* and then grown without leukemia inhibitory factor (LIF) for 3–4 days. Quantitative RT-PCR examination showed that *Gata4* and *Pdgfra* mRNAs (essential for primitive endoderm formation) were markedly suppressed in $Mob1a^{\Delta/\Delta}1b^{tr/tr}$ EBs, whereas *Cdx2* and *Eomesodermin* mRNAs (essential for TE) were only slightly inhibited (Figure 1C). Levels of *Oct3/4* (*Pou5f1*) and *Sall4* mRNAs (essential for ICM), as well as *Nanog*, *Fgf5*, *Pax6*, and *Sox2* mRNAs (essential for primitive ectoderm), were normal in the double-mutant EBs. Immunostaining of double-mutant blastocysts with antibodies recognizing CDX2 or Troma-1 (TE markers), NANOG or SOX2 (primitive ectoderm markers), or Oct3/4 confirmed that the levels of these proteins were also normal in the absence of *Mob1*. However, levels of GATA4 and PDGFRA proteins (primitive endoderm markers) were greatly reduced in the mutants (Figure 1D). Moreover, YAP1, which is usually expressed only in the nuclei of TE cells, was abnormally activated and expressed in the nuclei of ICM cells (Figure 1D). Thus, $Mob1a^{\Delta/\Delta}1b^{tr/tr}$ embryos have a defect in primitive endoderm formation.

$Mob1a^{\Delta/+}1b^{tr/tr}$ and $Mob1a^{\Delta/\Delta}1b^{tr/+}$ mice show increased susceptibility to tumorigenesis. $Mob1a^{\Delta/+}1b^{tr/tr}$ and $Mob1a^{\Delta/\Delta}1b^{tr/+}$ mice were born alive and were healthy and fertile, but 52% of them had dental malocclusion (Supplemental Figure 2A). In addition, 25% of these heterozygotes exhibited disequilibrium due to disorganized inner ear hair bundles in the cochlear organ of Corti (Supplemental Figure 2B and Supplemental Video 1), and 31% showed histological evidence of increased trabeculae in femurs (Supplemental Figure 2C).

Because mutation or reduced expression of *MOB1A* occurs in cancer patients (33), we monitored tumorigenesis in $Mob1a^{\Delta/+}1b^{tr/tr}$, $Mob1a^{\Delta/\Delta}1b^{tr/+}$, and $Mob1a^{\Delta/+}1b^{tr/+}$ (control) mice over 70 weeks. Various tumor types arose spontaneously in 100% of $Mob1a^{\Delta/+}1b^{tr/tr}$ and $Mob1a^{\Delta/\Delta}1b^{tr/+}$ mice, but in only 4% of controls (Figure 2, A and B, and Table 2). Southern blotting confirmed the loss of the WT *Mob1* allele in all tumors (Figure 2C). In most mutants, skin tumors in the form of facial swellings (Figure 2A) were observed. Benign exos-

Table 1
Viability of embryos of the indicated *Mob1a* genotypes from $Mob1a^{\Delta/+}1b^{tr/tr}$ intercrosses at the indicated stages of embryogenesis

		Genotype of *Mob1a*			
	Total	+/+	Δ/+	Δ/Δ	Absorbed
Viable	108	39	69	0	
E16.5	3	1	2	0	
E14.5	15	4	11	0	
E10.5	19	8	9	0	2
E9.5	27	11	13	0	3
E7.5	19	3	12	0	4
E6.5	47	11	23	0	13
E3.5	33	9	16	0	0

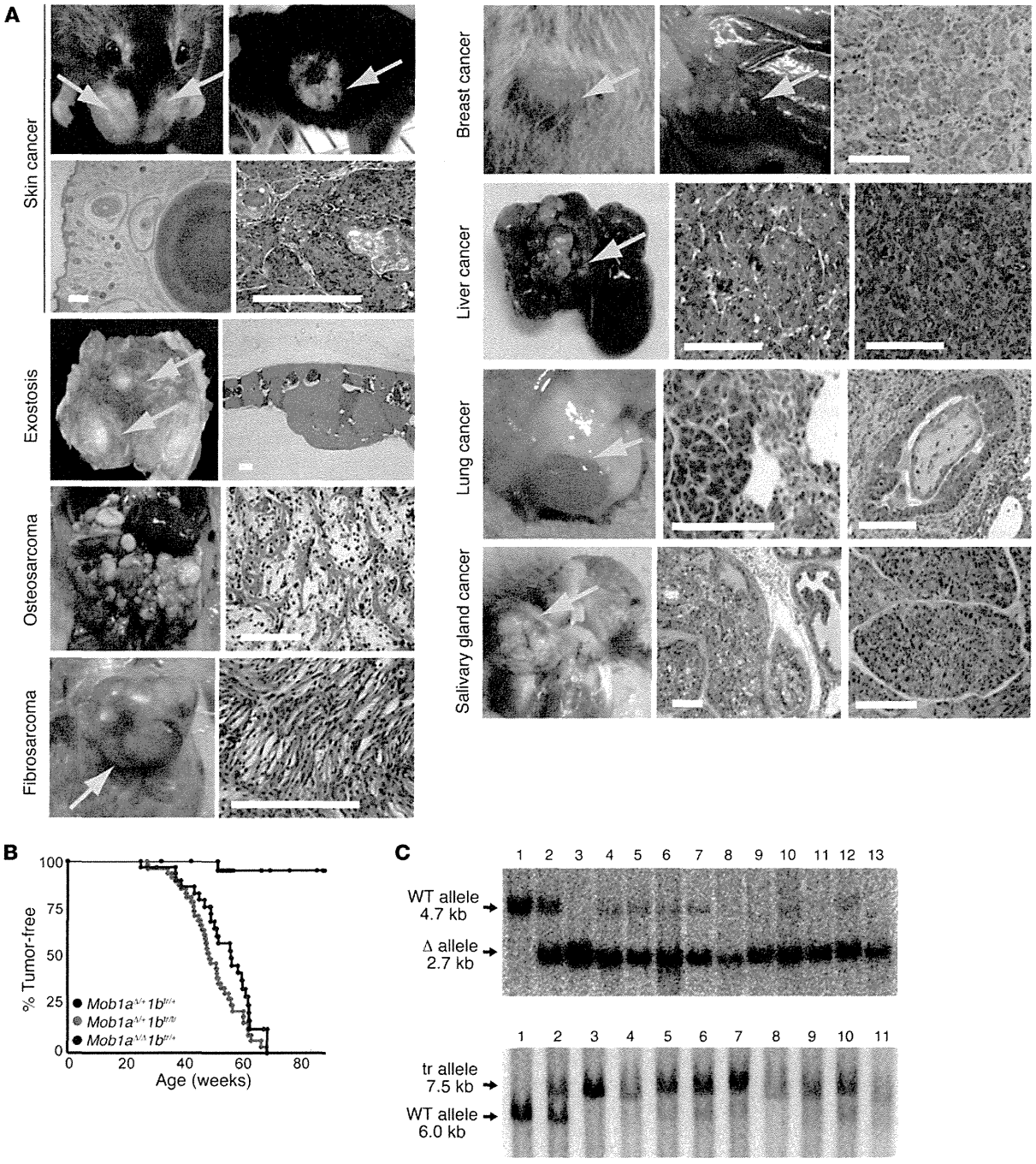

Figure 2

Loss of *Mob1a/1b* promotes tumorigenesis. (**A** and **B**) Tumor types arising in $Mob1a^{\Delta/\Delta}1b^{tr/+}$ or $Mob1a^{\Delta/+}1b^{tr/tr}$ mice. (**A**) Macroscopic or microscopic photographs of the indicated gross or H&E-stained tumors in mutant mice. Yellow arrows, tumor masses. Scale bars: 100 μm. (**B**) Kaplan-Meier analysis of tumor onset and survival for the $Mob1a^{\Delta/\Delta}1b^{tr/+}$ ($n = 31$), $Mob1a^{\Delta/+}1b^{tr/tr}$ ($n = 48$), and control $Mob1a^{\Delta/+}1b^{tr/+}$ ($n = 22$) mice in **A**. (**C**) Southern blots of tumor DNA showing loss of the WT *Mob1* allele. Top (hybridized to probe A of Supplemental Figure 1A): lanes 1–3, control thymic DNA from $Mob1a^{+/+}$, $Mob1a^{\Delta/+}$, and $Mob1a^{\Delta/\Delta}$ mice, respectively; lanes 4–5, osteosarcomas; 6–7, fibrosarcomas; 8–9, skin cancers; 10–11, breast cancers; 12–13, salivary gland cancers of $Mob1a^{\Delta/+}1b^{tr/tr}$ mice. Bottom (probe C): 1–3, control tail DNA of $Mob1b^{+/+}$, $Mob1b^{tr/+}$, and $Mob1b^{tr/tr}$ mice, respectively; 4–5, osteosarcomas; 6–7, fibromyosarcomas; 8–9, skin cancers; 10–11, liver cancers of $Mob1a^{\Delta/\Delta}1b^{tr/+}$ mice. Results shown are representative of at least 3 independent trials and at least 3 mice/group. Data are presented as the mean ± SEM, and *P* values were determined using the 2-tailed Student's *t* test.

Table 2
Total tumor numbers (incidence) for the mice in Figure 2A

	Mob1a$^{\Delta/+}$*1b*$^{tr/tr}$	*Mob1a*$^{\Delta/\Delta}$*1b*$^{tr/+}$	Overall
Skin cancer	23 (100%)	14 (100%)	37 (100%)
Exostosis	20 (87%)	14 (100%)	34 (92%)
Osteosarcoma	7 (30%)	2 (14%)	9 (24%)
Fibrosarcoma	6 (26%)	2 (14%)	8 (22%)
Liver cancer	0 (0%)	7 (50%)	7 (19%)
Breast cancer	5 (22%)	1 (7%)	6 (16%)
Lung cancer	0 (0%)	2 (14%)	2 (5%)
Salivary gland cancer	1 (4%)	1 (7%)	2 (5%)

tosis in calvaria occurred in 92% of animals with just 1 WT *Mob1* allele as well as extraskeletal osteosarcomas (24%), subcutaneous fibrosarcomas (or myofibrosarcomas) (22%), breast cancers (16%), lung cancers (5%), and salivary gland cancers (5%). Liver cancers were found only in *Mob1a*$^{\Delta/\Delta}$*1b*$^{tr/+}$ mutants (50%). Interestingly, none of our Mob1-deficient mice developed colon tumors or melanomas, unlike MOB1A-deficient humans (17, 33). Nevertheless, MOB1 is a powerful tumor suppressor in multiple tissues in vivo.

Keratinocyte-specific Mob1a/1b-deficient mice show gross skin abnormalities and die during lactation. Because the dominant tumor in *Mob1a*$^{\Delta/+}$*1b*$^{tr/tr}$ and *Mob1a*$^{\Delta/\Delta}$*1b*$^{tr/+}$ mice arose in the skin, we generated tamoxifen-inducible, keratinocyte-specific *Mob1a/1b* double-homozygous mutant mice (*Krt14CreERMob1a*$^{fl/fl}$*1b*$^{tr/tr}$). The *Keratin-14* (*Krt14*) promotor directs gene expression in the basal layer of epidermal and follicular keratinocytes, including stem cells in the HF bulge. Thus, tamoxifen-induced, *Krt14*-controlled Cre-mediated deletion of a floxed gene disrupts expression of that gene throughout the IFE and HFs (35). When we administered tamoxifen to *Krt14CreERMob1a*$^{fl/fl}$*1b*$^{tr/tr}$ mice at P1, we created double-homozygous conditional mutant mice [*k*DKO(P1)] that initially appeared healthy. Single-mutant mice (*Krt14CreERMob1a*$^{fl/fl}$*1b*$^{tr/tr}$) without tamoxifen or *Krt14CreERMob1a*$^{fl/fl}$*1b*$^{+/+}$ mice with tamoxifen were indistinguishable from the WT in gross appearance, histology, and survival (data not shown), allowing us to choose *Krt14CreERMob1a*$^{fl/fl}$*1b*$^{tr/tr}$ mice without tamoxifen as controls. Southern blotting confirmed that tamoxifen disrupted the *Mob1a*^{flox} allele in almost all keratinocytes of *k*DKO(P1) mice, leaving the *Mob1a*$^{\Delta}$ allele (Supplemental Figure 3A). In addition, immunostaining using an Ab recognizing both MOB1A and MOB1B (Supplemental Figure 3B) confirmed that the MOB1A and MOB1B proteins are expressed both in IFE cells (especially in the granular layer) and in HF cells (especially in matrix cells and outer root sheath cells) in normal mice and humans (Supplemental Figure 3, C and D). In contrast, MOB1A and MOB1B proteins were not detected in the epidermis of *k*DKO(P1) mice (Supplemental Figure 3C).

By 13 days of age, *k*DKO(P1) mice were significantly smaller than control littermates and readily identified by their "wrinkled-bear" facial skin (Figure 3A) and ruffled hair (Figure 3A). These mutants' front paws (Figure 3A), ears, and lips were hyperplastic and enlarged. All *k*DKO(P1) mice died of malnutrition within 10–30 days of birth (Figure 3), likely due to dysphagia caused by hyperplasia of the oral cavity epithelium.

We next analyzed the architecture of *k*DKO(P1) skin at various time points after birth. In WT mice, dividing keratinocytes are restricted to the basal epidermal layer. As these cells exit the cell cycle, they differentiate to form the spinous and granular skin layers as well as the dead, enucleated stratum corneum layers. The anagen phase of hair development thickens the skin until day 17, when the first catagen phase is triggered and skin thickness regresses until day 19. Hair remodeling then begins its lifelong cycle of spontaneous regrowth and regression (36). We saw this pattern clearly in our biopsy series from control mice (Supplemental Figure 4). However, the IFE and HFs of *k*DKO(P1) mice showed hyperplastic multilayered epithelium at day 16 (Figure 3B), and impaired epidermal regression during catagen (Supplemental Figure 4; day 19). In addition, parakeratosis (reduced enucleation) was evident in the stratum corneum layer of *k*DKO(P1) mice (Figure 3C).

To investigate keratinocyte differentiation, we used immunostaining to detect keratin markers in the fat pad epidermis, which allows easy analysis of epidermal layers. Keratin-15$^+$ (KRT15$^+$) cells, the most primitive in IFE, normally form a single basal layer attached to the IFE basement membrane (BM). This configuration was clearly visible in our controls, whereas the KRT15$^+$ cells of *k*DKO(P1) mice, although nearly normal in number, were scattered inside the IFE without attachment to the BM (Figure 3D). In control mice, KRT14$^+$ and KRT5$^+$cells were present in 1 or 2 IFE layers (as expected), but appeared in multiple layers in *k*DKO(P1) mice (Figure 3D). Moreover, there were increased numbers of irregularly organized KRT10$^+$ cells in the suprabasal layers of *k*DKO(P1) epidermis (Figure 3D). Filaggrin$^+$ cells, the most highly differentiated keratinocytes, were present in *k*DKO(P1) epidermis but at a reduced percentage (Figure 3D). Similar IFE alterations were observed in the back skin of *k*DKO(P1) mice (Figure 3E and Supplemental Figure 5). KRT17$^+$ outer root sheath cells were significantly increased in back skin HFs of *k*DKO(P1) mice, and Trichohyalin$^+$ inner root sheath cells were elevated slightly (Figure 3E). Thus, the phenotype of *k*DKO(P1) mice may be largely due to abnormal expansion of immature stem/progenitor skin cells.

To try to overcome the early lethality of *k*DKO(P1) mice, we waited until *k*DKO mice reached 28 days of age before treating them with tamoxifen for 7 days. However, like *k*DKO(P1) mice, all of these *k*DKO(P28) mice showed keratinocyte hyperplasia (Figure 3F) and died within 15–55 days after treatment (Supplemental Figure 6). Thus, MOB1 deficiency in epidermal cells severely disrupts normal IFE and HF development and homeostasis.

Tumorigenic anomalies in Mob1a/1b double-homozygous mutant keratinocytes. To determine whether loss of MOB1 conferred tumorigenic properties on keratinocytes, we first immunostained *k*DKO(P1) skin with anti-Ki67 Ab and found increased numbers of Ki67$^+$ proliferating epithelial cells (Figure 4A). In control mice at P13, a few Ki67$^+$ cells were located among basal IFE cells and outer root sheath cells, with more scattered among HF matrix cells. However, the incidence of Ki67$^+$ cells in *k*DKO(P1) skin at P13 was 1.5 times higher than in controls, and Ki67$^+$ cells were also found in the suprabasal layers normally quiescent in control epidermis. In addition, TUNEL-positive apoptotic cells were reduced in *k*DKO(P1) epidermis (Figure 4B). Thus, increased proliferation and repressed apoptosis may contribute to *k*DKO(P1) epidermal hyperplasia. Cell-plating studies revealed that the saturation density of *k*DKO(P1) keratinocytes was also increased (Figure 4C). Because the cell size (forward scatter) of control and mutant keratinocytes showed no difference by FACS analysis (data not shown), the increased saturation density of the mutant suggests impaired contact inhibition. Histological analysis confirmed that the mutant basal epidermal layer showed significantly increased cell density

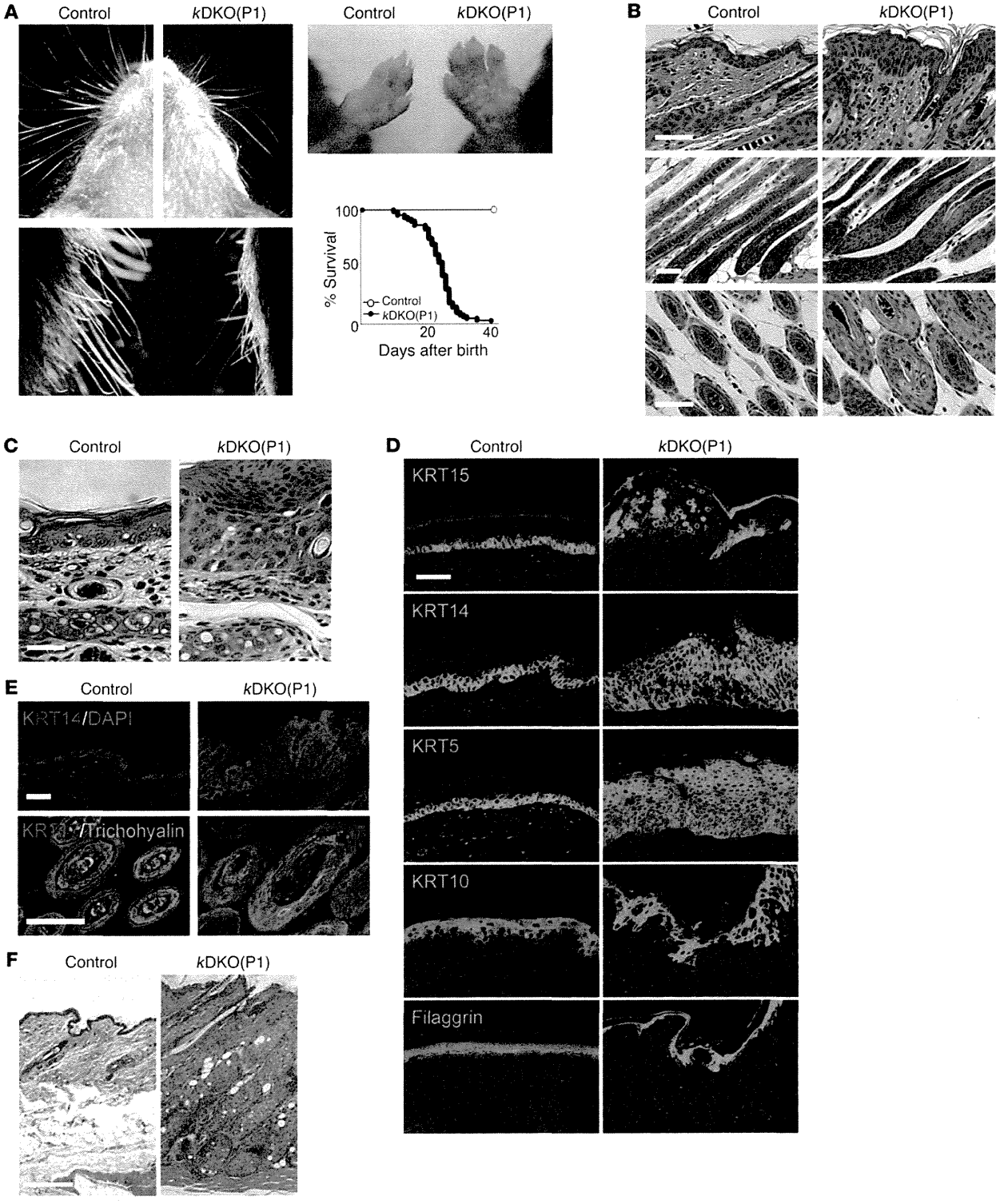
A
Control
kDKO(P1)
Control
kDKO(P1)
100
50
0
% Survival
Control
kDKO(P1)
20
40
Days after birth
B
Control
kDKO(P1)
C
Control
kDKO(P1)
D
Control
kDKO(P1)
KRT15
KRT14
KRT5
KRT10
Filaggrin
E
Control
kDKO(P1)
KRT14/DAPI
KRT1/Trichohyalin
F
Control
kDKO(P1)

Figure 3
Characterization of keratinocyte-specific *Mob1a/1b* double-homozygous mutant mice. (**A–C**) Features of 16-day-old *Krt14CreERMob1a*$^{fl/fl}$*1b*$^{tr/tr}$ mice that were originally left untreated (control) or treated with tamoxifen (*k*DKO) at P1. (**A**) *k*DKO(P1) mice have a wrinkled-bear facial appearance (top left), ruffled, shaggy body hair (bottom left), abnormally large front paws (top right), and decreased survival (bottom right). (**B**) H&E-stained longitudinal and transverse sections of the back skin of the mice in **A**. *k*DKO(P1) mice show hyperplasia of IFE and HF. Scale bars: 50 μm. (**C**) *k*DKO(P1) mice show parakeratosis (reduced enucleation) in stratum corneum layers. Scale bar: 20 μm. (**D**) Immunohistochemical analyses of fat pad epidermis of the mice in **A** using Alexa Fluor 488–tagged Abs recognizing the indicated differentiation markers corresponding to a specific skin layer. DAPI, nuclei. Scale bar: 50 μm. (**E**) Immunohistochemical analyses of back skin of the mice in **A** using Abs recognizing the indicated skin layer markers. For top panels, cells were stained with Alexa Fluor 568–tagged anti-KRT14 Ab. DAPI, nuclei. Scale bars: 20 μm. For bottom panels, cells were stained with Alexa Fluor 488–tagged anti-Trichohyalin Ab and Fluor 568–tagged anti-KRT17 Ab. Scale bar: 50 μm. (**F**) H&E-stained longitudinal sections of skin from 42-day-old *Krt14CreERMob1a*$^{fl/fl}$*1b*$^{tr/tr}$ mice that were left untreated (control) or treated with tamoxifen (*k*DKO) at P28. The *k*DKO(P28) mutant shows hyperplasia of IFE and HFs. Scale bar: 200 μm. Results shown are representative of at least 3 independent trials and at least 3 mice/group. Data are presented as the mean ± SEM.

(control: 7.6 ± 0.36 nuclei per 50 μm BM; mutant: 8.9 ± 0.38 nuclei per 50 μm BM; $n = 5$; $P < 0.05$). Morphologically, mutant basal cells were elongated and columnar rather than round like control basal cells (Figure 4D), also indicating defective contact inhibition.

Because yeast *MOB1* regulates mitotic exit and cytokinesis (24–29), we speculated that mammalian MOB1 might affect processes that support cell division. Indirect immunofluorescence analysis of control and *k*DKO(P1) keratinocytes using anti–γ-tubulin and anti–α-tubulin Abs revealed an increase in centrosome number (>2 centrosomes/cell) (Figure 4E). Aberrant centrosome numbers are associated with multipolar spindle formation that impairs chromosome segregation. Indeed, a greater percentage of *k*DKO(P1) keratinocytes exhibited multi-polar spindles (Figure 4F). Micronuclei, which are cytoplasmic chromosomal fragments generated by aberrant mitosis, were also increased in *k*DKO(P1) keratinocytes (Figure 4G). Similar defects were observed in *Mob1a* and *Mob1b* double-homozygous mutant embryonic fibroblasts (MEFs) (Supplemental Figure 7, A–C).

To determine which mitotic stage was altered in *k*DKO(P1) keratinocytes, we divided the mitotic process into 4 parts based on cell morphology: part I, cells progressing from the round morphology of a resting cell to chromosome alignment (corresponding to prometaphase); part II, from chromosome alignment to ingression of the cleavage furrow (metaphase/late anaphase); part III, from ingression to furrow completion (late anaphase/telophase); and part IV, from furrow completion to cell division (cytokinesis). We used time-lapse video microscopy to measure the duration of each of parts I–IV in control and *k*DKO(P1) keratinocytes. Part IV was significantly accelerated in MOB1-deficient cells compared with controls, while part I was slightly faster in the mutant (Supplemental Figure 8, A and B). No significant differences were detected for parts II and III. Thus, loss of MOB1 accelerates a cell's exit from mitosis.

We noted that *k*DKO(P1) mice had an apparent increase in the number of skin progenitors in the IFE (Figure 3D). We therefore performed RT-PCR to evaluate stem/progenitor cells in the HFs. CD34$^+$ and LGR6$^+$ cells are the most immature HF stem cells located in the bulge and isthmus. We found that *Cd34* and *Lgr6* mRNAs were normal or reduced in *k*DKO(P1) keratinocytes, but that markers of activated stem/progenitor cells, such as *Sox9* and *Lgr5*, were elevated (Figure 4H). These findings were confirmed by FACS analysis and immunohistochemistry (Figure 4H). However, despite their normal numbers, CD34$^+$ cells in mutant HFs could not localize to the proper bulge area (Supplemental Figure 9). This result mirrors the failure of HF stem cells to localize to the basal cell layer in MOB1-deficient IFE and HFs (Figure 3D). In addition, SOX9$^+$ cells (which are normally located in the bulge at P21) were markedly increased among *k*DKO(P1) keratinocytes and scattered throughout the HFs (Figure 4H). To determine how MOB1 inactivation affected HF stem cell self renewal, we quantified the ability of the total *k*DKO(P1) keratinocyte population to form colonies in culture. A lack of MOB1 induced a 2.1-fold increase in colony-forming efficiency (Figure 4I). When these primary colonies were replated to test their ability to form secondary colonies, a 3.0-fold increase in secondary colony-forming efficiency was observed in the absence of MOB1 (Figure 4I). Thus, MOB1 inactivation enhances the self renewal of activated stem/progenitor keratinocytes. This property, along with hyperproliferation, apoptotic resistance, impaired contact inhibition, increased centrosome number, and accelerated mitotic exit, may account for the frequent cancers observed in *Mob1*-deficient mice.

MOB1-mediated regulation of the LATS1/2-YAP1 pathway controls skin homeostasis. To characterize the mechanisms driving the *k*DKO(P1) phenotype, we investigated the effects of MOB1 loss on signaling mediated by YAP1 and its upstream kinases LATS1/2. In vitro, MOB1 is important for the full activation of LATS kinases (37), and activated LATS1/2 phosphorylate YAP1 and inhibit its nuclear localization (38). Using immunohistochemistry, we found that, in control mice, YAP1 was localized in the nuclei of most outer root sheath cells, in some HF matrix cells, and in some IFE basal cells (Figure 5A). However, *k*DKO(P1) mice exhibited not only greater numbers of nuclear YAP1$^+$ cells in these sites but also some nuclear YAP1$^+$ cells in the upper IFE layer (Figure 5A). Immunoblotting of keratinocytes confirmed that the phosphorylation of YAP1 on Ser127 was reduced, but that total YAP1 was increased in the absence of MOB1 (Figure 5B), especially in the nucleus (Figure 5C). When we cultured keratinocytes under high cell density conditions, YAP1 was inactivated and localized in the cytoplasm in control cells (Figure 5D). In contrast, in *k*DKO(P1) keratinocytes, YAP1 remained activated and positioned in the nucleus even at high-cell density (Figure 5D). Thus, MOB1 is required for density-induced subcellular localization of YAP1.

We next investigated LATS1/2 phosphorylation in control and mutant keratinocytes. Immunoblotting demonstrated that, in the absence of any stimulation, levels of phospho-LATS1(T1079) and phospho-LATS2(T1041) were below the assay detection limit even in control keratinocytes (Figure 5E). We then stimulated control and *k*DKO(P1) keratinocytes with okadaic acid (OA), which activates the MST kinases acting upstream of LATS1/2 (39). While OA-stimulated control keratinocytes showed vigorous phosphorylation of LATS1/2, OA-stimulated *k*DKO(P1) keratinocytes did not. Strikingly, total LATS1/2 protein levels were also reduced in the mutant. This inhibition of LATS1/2 phosphorylation was not due solely to the reduction in total LATS1/2 proteins because levels of phospho-LATS1/2 were also markedly decreased when total LATS1/2 protein levels in each sample were adjusted to equality prior to electropho-

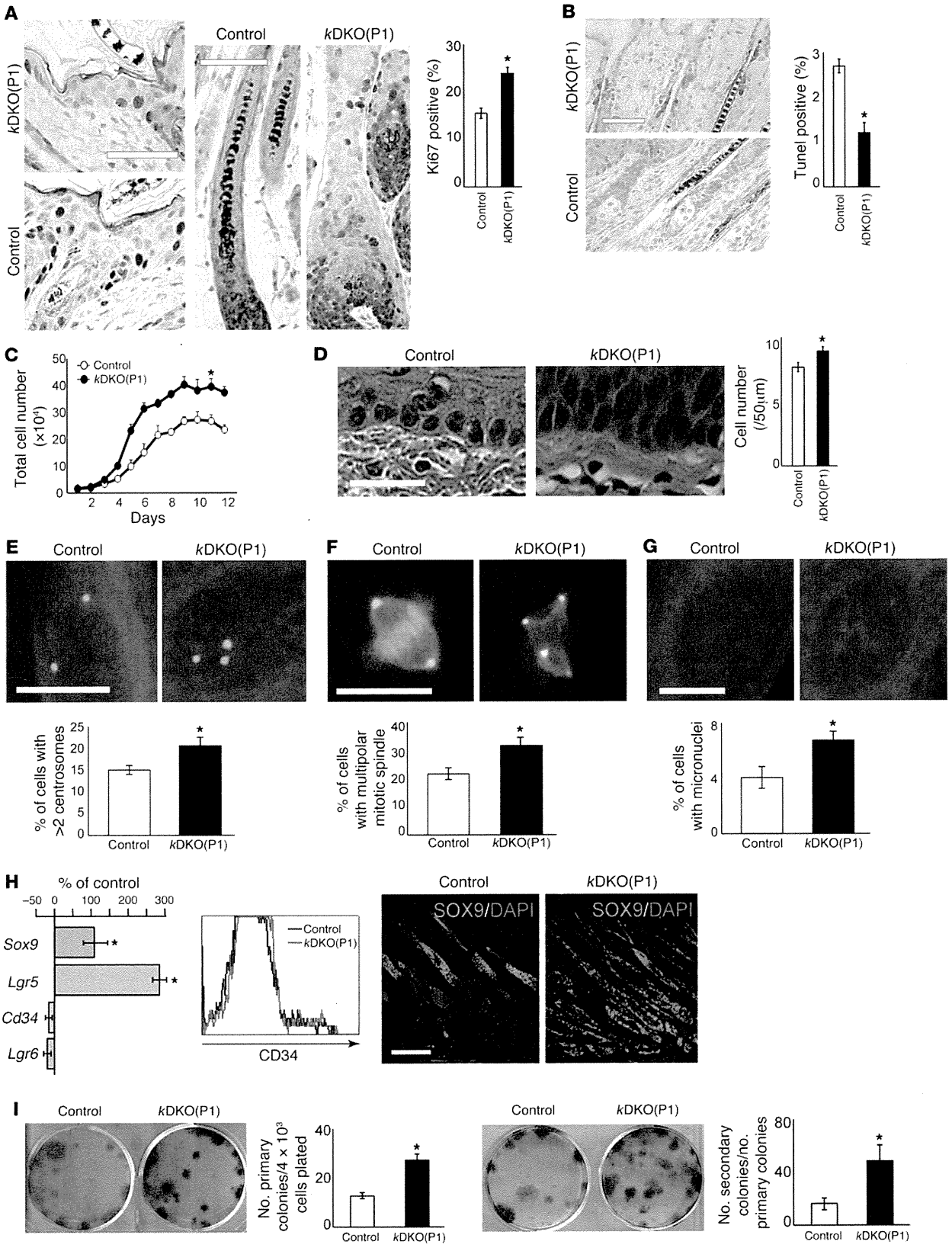
A
Control
kDKO(P1)
kDKO(P1)
Control
Ki67 positive (%)
B
kDKO(P1)
Control
Tunel positive (%)
C
Control
kDKO(P1)
Total cell number (×10⁴)
Days
D
Control
kDKO(P1)
Cell number (/50μm)
E
Control
kDKO(P1)
% of cells with >2 centrosomes
F
Control
kDKO(P1)
% of cells with multipolar mitotic spindle
G
Control
kDKO(P1)
% of cells with micronuclei
H
% of control
Sox9
Lgr5
Cd34
Lgr6
Control
kDKO(P1)
CD34
Control
kDKO(P1)
SOX9/DAPI
SOX9/DAPI
I
Control
kDKO(P1)
No. primary colonies/4 × 10³ cells plated
Control
kDKO(P1)
No. secondary colonies/no. primary colonies